Universal correlation between H-linear magnetoresistance and T-linear resistivity in high-temperature superconductors

J Ayres, M Berben, C Duffy, R D H Hinlopen, Y-T Hsu, A Cuoghi, M Leroux, I Gilmutdinov, M Massoudzadegan, D Vignolles, et al.

nature communications

Article

https://doi.org/10.1038/s41467-024-52564-3

Universal correlation between *H*-linear magnetoresistance and *T*-linear resistivity in high-temperature superconductors

Received: 24 May 2024

Accepted: 10 September 2024

Published online: 27 September 2024

Check for updates

J. Ayres[1,9] ✉, M. Berben[2,9], C. Duffy[2,3], R. D. H. Hinlopen[1,4], Y.-T. Hsu[2,5], A. Cuoghi[2], M. Leroux[3], I. Gilmutdinov[3], M. Massoudzadegan[3], D. Vignolles[3], Y. Huang[6], T. Kondo[7], T. Takeuchi[8], S. Friedemann[1], A. Carrington[1], C. Proust[3] & N. E. Hussey[1,2] ✉

The signature feature of the 'strange metal' state of high-T_c cuprates—its linear-in-temperature resistivity—has a coefficient α_1 that correlates with T_c, as expected were α_1 derived from scattering off the same bosonic fluctuations that mediate pairing. Recently, an anomalous linear-in-field magnetoresistance ($=\gamma_1 H$) has also been observed, but only over a narrow doping range, leaving its relation to the strange metal state and to the superconductivity unclear. Here, we report in-plane magnetoresistance measurements on three hole-doped cuprate families spanning a wide range of temperatures, magnetic field strengths and doping. In contrast to expectations from Boltzmann transport theory, γ_1 is found to correlate universally with α_1. A phenomenological model incorporating real-space inhomogeneity is proposed to explain this correlation. Within this picture, superconductivity in hole-doped cuprates is governed not by the strength of quasiparticle interactions with a bosonic bath, but by the concentration of strange metallic carriers.

The temperature (T) and magnetic field (H) dependence of the electrical resistivity ρ of a metal contains a wealth of information on the dominant interactions that scatter the conduction electrons and thus can mediate superconducting (SC) pairing. In conventional metals, the T-linear electron-phonon (e-ph) scattering rate $\hbar/\tau_{ph} = 2\pi\lambda_{tr}k_BT$ where $\hbar$ is Planck's constant, k_B Boltzmann's constant and λ_{tr} is the e-ph coupling constant for transport. λ_{tr} is closely related to λ, the e-ph coupling strength used in the determination of T_c in BCS superconductors via the McMillan formula[1]; a correspondence which underlies the old adage 'good metals make bad superconductors'.

This correlation between λ_{tr} and T_c contrasts in an interesting way with what is found in certain quantum critical metals that also superconduct. In these materials, a fan-like region of T-linear resistivity, emanating from a quantum critical point (QCP), is attributed to scattering off critical fluctuations of the underlying order[2,3] that is strong enough to destroy the Fermi-liquid (FL) ground state. Empirically, both α_1 (the coefficient of the T-linear resistivity) and the extracted scattering rate $\hbar/\tau \sim \zeta k_BT$ ($1 \le \zeta \le \pi$) are approximately constant within the quantum critical fan[3,4] and as such, do not correlate with T_c. This lack of correlation supports the notion that inelastic scattering within the fan is bounded to a maximal equilibration rate for charge carriers known as the Planckian limit[5,6]. The notion of Planckian dissipation is now associated with a broad class of strongly interacting materials, including high-T_c cuprates[5,7,8], ultracold atoms[9] and twisted

[1]H. H. Wills Physics Laboratory, University of Bristol, Bristol, UK. [2]High Field Magnet Laboratory (HFML-EMFL) and Institute for Molecules and Materials, Radboud University, Nijmegen, Netherlands. [3]LNCMI-EMFL, CNRS UPR3228, Univ. Grenoble Alpes, Univ. Toulouse, INSA-T, Toulouse, France. [4]Max-Planck-Institute for the Structure and Dynamics of Materials, Hamburg, Germany. [5]Department of Physics, National Tsing Hua University, Hsinchu, Taiwan. [6]Van der Waals-Zeeman Institute, University of Amsterdam, Amsterdam, Netherlands. [7]Institute for Solid State Physics, University of Tokyo, Kashiwa, Japan. [8]Toyota Technological Institute, Nagoya 468-8511, Japan. [9]These authors contributed equally: J. Ayres, M. Berben. ✉e-mail: jake.ayres@bristol.ac.uk; n.e.hussey@bristol.ac.uk

bilayer graphene[10], motivating the search for a unified explanation with[11,12] or without well-defined quasiparticles[13,14].

In overdoped cuprates, the low-T in-plane resistivity is empirically well described by $\rho_{ab}(T) = \rho_0 + \alpha_1 T + \beta T^2$ where α_1 is finite not at a singular point but over an extended doping range—from just beyond optimal doping to the edge of the SC dome[7,15]. Such extended T-linearity to the lowest T is suggestive of a quantum critical *phase*[14,16] and is a defining characteristic of the cuprate 'strange metal' regime[17]. In marked contrast to what is found in quantum critical metals, α_1 in overdoped cuprates is correlated with both T_c[7,15] and the superfluid density n_s[17]. At first sight, these correlations suggest an analogy with conventional BCS superconductors, with spin[18] or charge[19] fluctuations possibly playing the role of the scattering boson for transport and Cooper pair formation alike. The existence of an interacting boson of variable strength (i.e., variation in α_1), as well as the presence of a T^2 scattering rate, however, sit at odds with the notion of universal Planckian dissipation[8].

In order to gain further insights into the nature of the strange metal (SM) regime in cuprates, attention has switched to the magnetoresistance (MR) response at high fields ($20\ \mathrm{T} \le \mu_0 H \le 90\ \mathrm{T}$), specifically the robust H-linear MR observed in both electron-[20] and hole-doped cuprates[21–23]. To date, these high-field studies have tended to focus on a rather narrow, isolated region of their respective phase diagrams and as such, any attempt to find a relation between the H-linear MR and T-linear resistivity has been speculative. To address this, we have carried out a comprehensive high-field MR study on three hole-doped cuprate families: (Pb/La)-doped $Bi_2Sr_2CuO_{6+\delta}$ (Bi2201), $Tl_2Ba_2CuO_{6+\delta}$ (Tl2201) and $La_{2-x}Sr_xCuO_4$ (LSCO) for which the correlation between α_1 and T_c is well established[7,24,25]. Our study reveals a striking and robust correlation between α_1 and γ_1, the slope of the high-field H-linear MR. A simple, phenomenological model is proposed that is able to account both for the $(T + T^2)$ form of the resistivity and for the non-trivial correlation between α_1 and γ_1. When combined with the correlation between α_1, T_c and n_s, we conclude that weakening superconductivity in overdoped cuprates is governed not by a decreasing strength of quasiparticle interactions, but by a reduction in the number of strange metallic (possibly Planckian) carriers.

Results

Panels (a–e) of Fig. 1 show $\rho(H, T)$ for a representative set of Bi2201 single crystals over a wide doping range that incorporates both the pseudogap ($0.13 \le p < p^* \sim 0.20$) and strange metal ($p^* < p \le 0.27$) regimes. (In all measurements shown here, the current I is applied within the CuO_2 plane and $\mathbf{H} \parallel c$). In highly doped samples with a low T_c, the crossover from quadratic to linear MR is clearly visible within the accessible field range. At lower dopings where T_c is elevated, the low-T behaviour is obscured by superconductivity and only H-linearity is observed at high fields. At higher T, the MR is predominantly quadratic but approaches linearity at high fields with a coefficient in agreement with the data reported over a much more limited field and doping range in ref. 22. In all cases, H-linearity is asymptotically approached at the highest fields.

The red shaded regions of panels (a–e) highlight the doping evolution of the MR at a fixed temperature $T = 80$ K that in all cases lies well above the temperature below which paraconductivity contributions from SC fluctuations become apparent. Noting that the absolute span in ρ is the same (140 $\mu\Omega$cm) in all panels, it is evident that the magnitude of the MR decreases monotonically with increasing p. The overall trend is summarized in Fig. 1f where $\Delta\rho(H, 80\ \mathrm{K}) = (\rho(H, 80\ \mathrm{K}) - \rho(0, 80\ \mathrm{K}))$ is plotted for 8 different dopings. $\rho(0, 80\ \mathrm{K})$ itself decreases roughly by a factor of 2 across the series, reflecting changes in the scattering rate and/or the carrier density. $\Delta\rho(H, 80\ \mathrm{K})$, by contrast, decreases by more than one order of magnitude. The corresponding $\Delta\rho(H, 80\ \mathrm{K})/\rho(0, 80\ \mathrm{K})$ values are plotted in Fig. 1g. Intriguingly, for the three samples in the pseudogap regime with $p < p^*$ (~0.2), $\Delta\rho(H, 80\ \mathrm{K})/\rho(0, 80\ \mathrm{K})$ is found to be independent of doping. The same is also seen in LSCO below p^*—see Supplementary Fig. 3c. This implies that the increase in $\Delta\rho$ below p^* is a direct consequence of the increase in $\rho(0)$ with underdoping, presumably due to the loss of electronic states once the pseudogap opens. For higher dopings, by contrast, even the fractional change in MR is found to vary strongly with p, decreasing by one order of magnitude between $p = 0.205$ and 0.27 (see Fig. 1g).

At high H/T (below T_c in most samples) and for all dopings, the MR asymptotically approaches H-linearity with a T-independent slope γ_1, as shown in ref. 22 and illustrated for $p = 0.205$ in Fig. 1h. In order to obtain estimates for $\gamma_1(p)$, we study the low-T limit of the highest field data (where the normal state can be accessed). A summary of the results is shown in Fig. 1i where the T-dependence of $\mathrm{d}\rho/\mathrm{d}\mu_0 H|_{H_{\max}}$—the MR slope at the highest measured field range (i.e. over the last 3 T of each field sweep)—is plotted for all the samples whose raw MR data are included in panels (a–e). In agreement with previous measurements on LSCO[21], $\mathrm{d}\rho/\mathrm{d}\mu_0 H|_{H_{\max}}$ is found to increase with decreasing T and to saturate at a constant value ($=\gamma_1$) at low T. As a function of doping, $\gamma_1(p)$ exhibits a monotonic decrease, consistent with our expectations from Fig. 1g.

Two further studies were conducted: one on a single crystal of overdoped Tl2201 ($T_c = 35$ K at ambient pressure) as a function of hydrostatic pressure and one on a series of LSCO single crystals, the data for which are reported in Supplementary Figs. 2 and 3, respectively. The T_c (and inferred doping) of Tl2201 can be tuned appreciably with the application of modest pressures[26]. A gradual decrease in γ_1 is observed with increasing pressure, consistent with the correlation between γ_1 and T_c (or p) seen in Bi2201 beyond p^*. As reported in ref. 21, LSCO near p^* ($x = 0.19$) also exhibits H-linear MR at the highest fields. Here, the MR of two LSCO samples with $x = p = 0.20$ and 0.23 up to 35 T has been measured and pulsed-field data reported in ref. 7 for $p = 0.17$ and 0.23 reanalysed. The field derivatives show clearly that, just as in Bi2201 and Tl2201, the MR becomes H-linear at high H/T values.

The results for all three families are summarised in Fig. 2; the left and right panels showing, respectively, the doping or pressure evolution of γ_1 and α_1. (Although an equivalence between pressure and hole doping in Tl2201 has not yet been definitively demonstrated, we adopt here the dependence of T_c on p reported in ref. 25 to arrive at the same conclusion). Despite the very different Fermi surface topologies, degree of electronic inhomogeneity and electron mobility across the three families, both α_1 and γ_1 exhibit a clear linear doping dependence and extrapolate to zero at the same doping concentration in all cases, implying a direct and robust correlation between the two. That both coefficients extrapolate to zero at a doping level $p \approx 0.3$ and positively correlate with T_c throughout the SM regime also implies that the emergence of H-linear MR and T-linear resistivity is closely tied to the onset of superconductivity. While previous studies[20–22] have hinted at a trend in γ_1, the doping ranges in each case were too narrow ($\Delta p \le 0.03$) to make any definitive claims.

Discussion

In order to understand why these correlations are non-trivial, let us first consider the MR response of a FL described by Boltzmann transport theory. Being an even function of H, the MR is always quadratic at the lowest field strengths, though it is the cyclotron frequency ω_c ($\propto H$), not τ, that sets the field dependence of $\Delta\rho(H)$. Its magnitude, on the other hand, is set primarily by the product $\omega_c\tau$ and its variation (anisotropy) over the Fermi surface. (Recall that MR vanishes in a perfectly isotropic metal[27]). Provided that this anisotropy does not vary significantly with temperature, the T-dependence of $\Delta\rho(H)$ will be determined largely by that of $\rho(T)$, as expressed through Kohler's rule: $\Delta\rho/\rho(0, T) = f(H/\rho(0, T))$. With increasing field strength, $\Delta\rho(H)$ will pass through an inflection point before saturating once multiple cyclotron orbits have washed out all manifestations of anisotropy. Hence, unless

https://doi.org/10.1038/s41467-024-52564-3

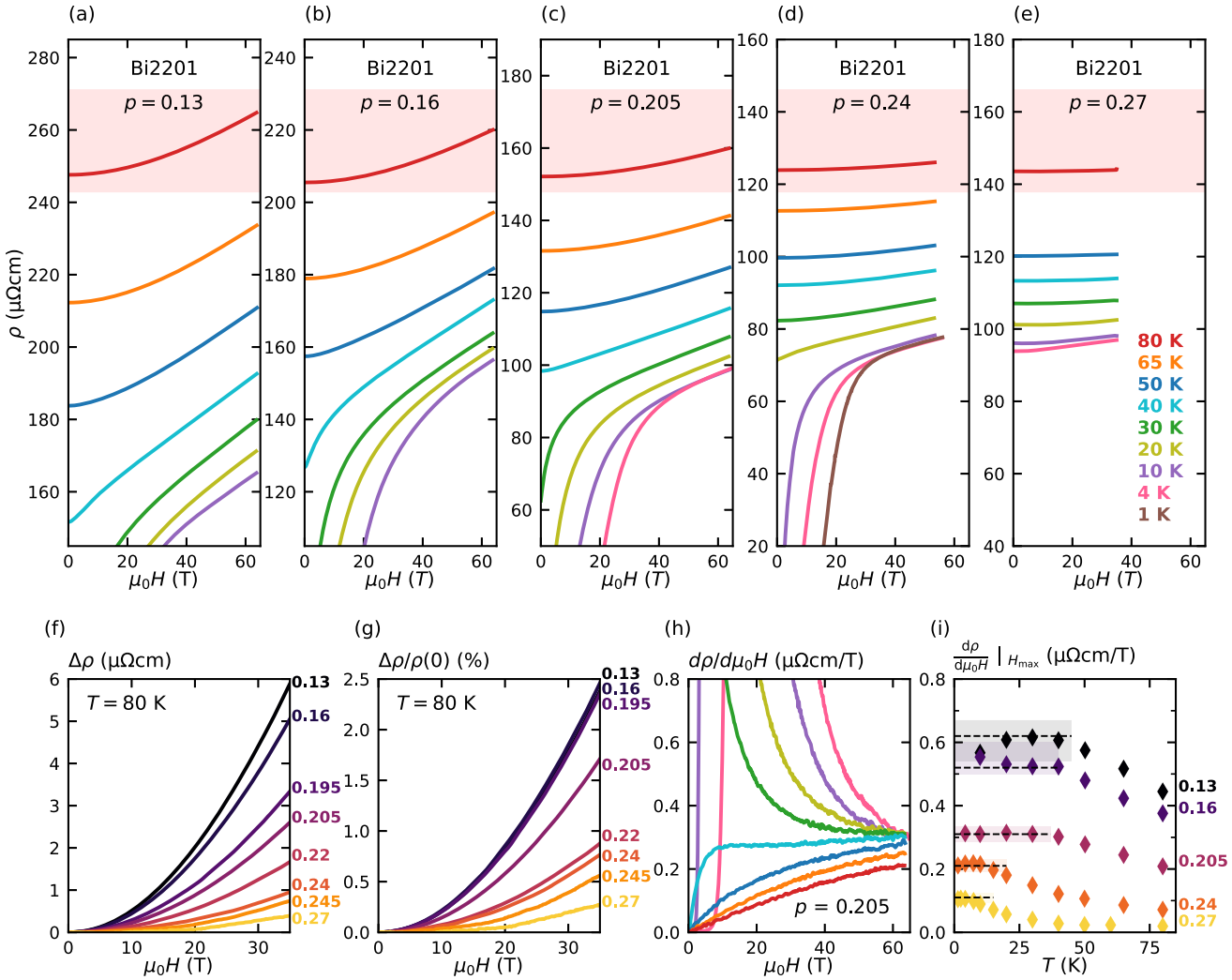

Fig. 1 | Doping dependence of the transverse MR in Bi2201. a–**e** $\rho(H, T)$ of selected Bi2201 crystals over the doping range $0.13 \le p \le 0.27$. With increasing p, a marked decrease in the magnitude of the MR (at a constant temperature) is observed, as highlighted by the red shaded regions for $T = 80$ K. **f** $\Delta\rho(H, 80\,\text{K})$ curves for 8 different dopings. **g** Corresponding $\Delta\rho/\rho(0)$ curves. For $p > p^* \sim 0.2$, the magnitude of $\Delta\rho/\rho(0)$ drops with increasing p, revealing that within the SM regime ($p^* < p < 0.27$), the order-of-magnitude enhancement in the MR is not a result of an increase in $\rho(0, T)$ (e.g. due to a reduced carrier density). **h** The derivative of the MR at $p = 0.205$ illustrating the tendency at all temperatures to H-linearity at high fields. The line colours are the same as those used in (**a**)–(**e**). **i** T-dependence of $d\rho/d\mu_0 H$ at the highest measured field range (specifically the last 3 T of each field sweep) for the MR curves displayed in (**a**)–(**e**). For all dopings, $d\rho/d\mu_0 H|_{H_{max}}$ saturates at low T at a value ($= \gamma_1$) denoted by horizontal dashed lines. Shaded regions reflect the uncertainty in γ_1 for each data set. Estimates for γ_1 obtained from field sweeps for which the H-linear regime could not be reached are not shown. For the optimally-doped sample ($p = 0.16$), the upturn in $d\rho/d\mu_0 H|_{H_{max}}$ at the lowest T is due to para-conductivity effects. The origin of the low-T downturn in $d\rho/d\mu_0 H|_{H_{max}}$ for $p = 0.13$ is unknown. Nevertheless, an estimate for γ_1 can still be made, albeit with greater uncertainty.

the anisotropy itself is extreme[28] or multiband effects are involved[29], no extended region of H-linear MR is expected.

With regards to the doping dependence, a decreasing magnitude of the MR due to a monotonic reduction in $\omega_c\tau$ at low-T as the system is doped away from the Mott insulating state (and thus becomes increasingly more metallic) seems unlikely; there is little variation in the residual resistivity ρ_0 within this doping range and no indication, e.g. from existing specific heat measurements[30,31], for a large change in m^*. Moreover, the magnitude of γ_1 in Bi2201 and Tl2201 is essentially the same, despite their ρ_0 values differing by almost one order of magnitude.

The alternative explanation—a reduction in the effective anisotropy of $\omega_c\tau$ with increasing p—could in principle apply to LSCO. Strong in-plane anisotropy in the elastic mean-free-path $\ell_0(\phi)$ has been deduced at a doping close to where the Fermi level crosses the van Hove singularity (vHs)[32] and shown to generate a broad regime of H-linear MR of the right order of magnitude[23]. Moreover, beyond the edge of the SC dome, this anisotropy in $\ell_0(\phi)$ is known to be much reduced[33]. As shown in Supplementary Fig. 4, however, incorporating the known Fermi surface geometry and a form of $\ell_0(\phi)$ that tracks the anisotropy in the density of states into the Boltzmann equation, we find that $\Delta\rho/\rho(0)$ and γ_1 are essentially doping independent across the SM regime, in marked contrast with experimental findings.

More constraining is the fact that in Bi2201, the vHs crossing point is located close to $p \sim 0.27$[34,35], i.e. where the MR is smallest, while in Tl2201, it is believed to be located at a doping level ($p \sim 0.54$) that is far higher than those studied here[25]. Hence, in both Bi2201 and Tl2201, one should expect anisotropy in $\ell_0(\phi)$ and the resultant MR to grow with increasing p (as confirmed in the simulations for Bi2201 plotted in Supplementary Fig. 5). Thus, given what is known about these three distinct families, the ubiquitous and marked decrease in γ_1 across the SM regime appears difficult to reconcile within any viable Boltzmann framework, even one incorporating a very specific combination of Fermiology and anisotropic scattering.

https://doi.org/10.1038/s41467-024-52564-3

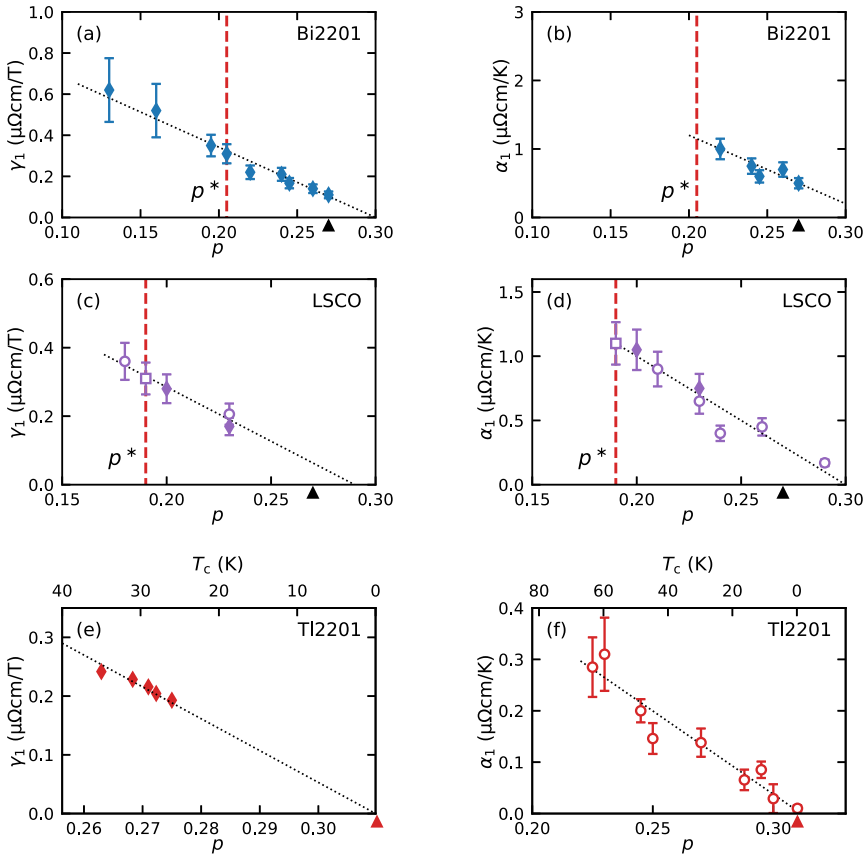

Fig. 2 | Universal correlation between γ_1 and α_1 in overdoped cuprates. Doping dependence of γ_1—the high H/T limiting value of the MR—and α_1—the low-T T-linear coefficient of the resistivity—for (**a**, **b**) Bi2201, (**c**, **d**) LSCO and (**e**, **f**) Tl2201, respectively. Diamonds indicate results obtained as part of this high-field study, while circles and squares indicate results obtained from the literature. Circles and squares in (**c**) and (**d**) are taken from refs. 7, 21, respectively. Circles in (**f**) are from ref. 24. Note that α_1 is plotted only for samples with $p > p^*$. In **e**, γ_1 is plotted vs. p as determined from the T_c value at each pressure using the correlation reported in ref. 25. Error bars on points marked as solid diamonds are due to geometric uncertainty in the absolute value of the resistivity and necessary extrapolations. Error bars on the open squares and circles are taken from the relevant source, if provided, or assumed to be 15% (typical uncertainty in the geometrical ratios) if not. In (**e**), no random uncertainty in contact geometry is present due to a single sample being measured but a systematic uncertainty of 20% is included. All dotted lines are guides to the eye. Arrowheads on the doping axes indicate p_{sc} for the respective material.

There are several other known mechanisms for generating a H-linear MR in metals, in particular, those that incorporate a random distribution in carrier density and mobility. As we discuss in the Supplementary Information Section IV, however, none of these seem capable of explaining the key observations: the H/T scaling of the MR in the presence of a large ρ_0, the correlation between α_1 and γ_1 and the presence of the T^2 component in $\rho(T)$ in a consistent manner. What is both intriguing and constraining here is the ubiquity of the H-linear MR (in multiple families with different Fermiologies), its magnitude, form and T-dependence and the aforementioned correlations (with α_1 and T_c).

One of the most striking features of the MR response in overdoped cuprates is its empirical adherence to the quadrature expression: $\rho(H, T) = \mathcal{F}(T) + \sqrt{(\alpha k_B T)^2 + (\gamma \mu_0 H)^2}$ [36], where α (γ) are the T- (H-) linear coefficients within the quadrature expression, respectively, and $\mathcal{F}(T) \sim \rho_0 + \beta T^2$ [22]. (Note here that the entire field response is encapsulated in the quadrature expression; the $\mathcal{F}(T)$ component itself possessing negligible MR.) An example of the applicability of this expression is shown for Tl2201 in Supplementary Fig. 2 (dashed lines). Such a decomposition of $\rho(H, T)$ may signify either the presence of two independent inelastic scattering rates (one T-linear, one quadratic) or two resistive channels coupled in series. For the former, these rates should combine with the elastic (impurity) scattering to generate a total scattering rate whose overall T-dependence is also reflected in the MR, an outcome that is inconsistent with the strict adherence to the quadrature expression (in which only the T-linear component of $\rho(T)$ appears in the MR). Secondly, the large value of ρ_0 in Bi2201 and the lack of sufficient k-space anisotropy in the mean-free-path ℓ in Tl2201 at low T [37] ensure that any MR calculated using Boltzmann transport theory and the known parameterization for each system is at least one order of magnitude smaller than what is seen in experiment. Given these empirical facts, we proceed by assuming that $\rho(H, T)$ is composed of two distinct sectors (phases) separated in real space, only one of which contributes significantly to the MR.

Overdoped cuprates have long been considered as systems exhibiting microscopic phase separation and granular superconductivity [38–40]. In Bi2201, for example, real-space patchiness has been imaged directly by STM for all dopings within the SM regime [41]. Patchiness has also been inferred for strongly overdoped LSCO [42]. Guided by this and the tendency for the magnetotransport to interpolate smoothly from pure FL-like behaviour (quadratic resistivity and small MR) at high dopings to pure SM behaviour (T-linear resistivity and large MR) near p^*, we apply effective medium theory (for which the granularity of the model is scale-invariant) to a network of distinct FL and non-FL patches.

According to this picture, a fraction f of the sample is assigned a strange metallic T-linear resistance while the remainder is assigned a FL quadratic resistance. The resistance of the sample for the two limiting cases where $f = 0$, 1 are shown in Fig. 3a. For intermediate f, the

https://doi.org/10.1038/s41467-024-52564-3

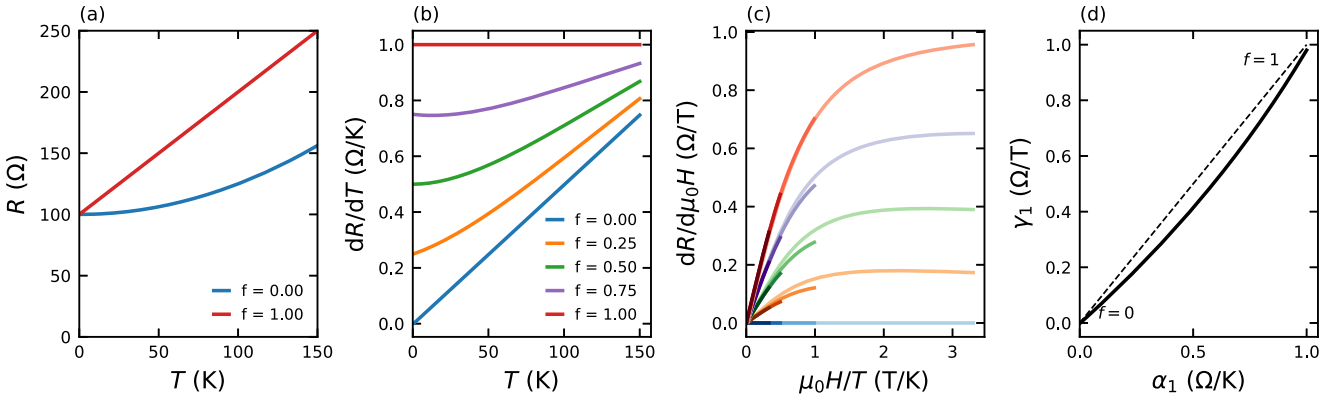

Fig. 3 | Modelling the doping dependence of the MR with effective medium theory. A fraction f of the sample is assumed to have a zero-field T-linear resistance and quadrature MR: $R_{SM} = 100 + \sqrt{T^2 + (\mu_0 H)^2}$. The remainder of the sample is assigned a FL resistance with no MR: $R_{FL}(T, B) = 100 + T^2$. The macroscopic resistance of the sample is then computed for various values of f using effective medium theory as described in ref. 43. **a** Resistance R of the sample in limiting cases where $f = 0, 1$. **b** Temperature derivative of the resistance dR/dT for different values of f. A systematic increase in α_1, the low-T T-linear coefficient of the resistance, is found with increasing f. **c** Field derivative of the sample resistance dR/dH plotted against H/T. With decreasing f, the quadrature MR intrinsic to the strange metallic part of the sample is diluted by an increasing fraction of the FL component. The scaling is reasonably well maintained for intermediate f. **d** The T-linear coefficient of the resistance α_1 is seen to correlate with γ_1—the H-linear slope of the high field MR—with both growing monotonically with increasing f.

macroscopic resistance is computed following[43]. This is already sufficient to reproduce a sample resistance that at low T has the observed $\alpha_1 T + \beta T^2$ form with α_1 smoothly increasing as a function of f (Fig. 3b). If one further assumes that the strange metal patches also have an intrinsic MR than scales with H/T (justified by the observed adherence to the quadrature form) and that the FL-like resistors have a negligible MR (in accordance with expectations from Boltzmann theory), one obtains an MR that retains H/T scaling reasonably well for all values of f (Fig. 3c) with a high-field H-linear slope γ_1 that correlates with α_1 (Fig. 3d).

Our phenomenological model, though overly simplistic, does appear to capture most, if not all, of the key observations: the low-T form of the resistivity ($\rho_0 + \alpha_1 T + \beta T^2$), the quadrature form of the MR and associated H/T scaling as well as the correlation between γ_1 and α_1 self-consistently. While the distinct patchwork picture introduced here is probably not by itself sufficient, we expect that real-space inhomogeneity of the type highlighted in this study will be an essential ingredient of any subsequent microscopic model. Distributed networks of metallic components have previously been invoked to explain the MR of both pnictides[44] (which also scales with H/T) and cuprates[45] at singular dopings where the resistivity is purely T-linear. 2D random resistor networks are capable of producing non-saturating H-linear MR by incorporating continuous resistivity or mobility disorder[46], while inhomogeneity in the carrier density can generate a similar MR response[47]. Moreover, an extension of the resistor network model to 3D returns a H-linear MR in longitudinal fields[48] as observed in both Tl2201 and Bi2201 for $\mathbf{H} \parallel ab$ and for which an explanation is currently lacking[22]. One salient property of this variety of model is that the resultant behaviour is insensitive to details of the Fermiology that (within a Boltzmann framework) should distinguish the various materials studied but appear not to. It remains a challenge, however, for such models to reproduce the H/T scaling, a feature that appears to set this particular MR response apart from all others.

In closing, our study has revealed a robust correlation between the coefficient α_1 of the T-linear resistivity and the H-linear slope of the high-field MR in three distinct families of hole-doped cuprates. It has been argued that such a universal correlation cannot be reconciled with any simple reformulation of Boltzmann transport theory. Although the present two-component model cannot account for all of the in-plane transport properties of overdoped cuprates[25], it nevertheless provides a basic framework that captures much of the essential phenomenology on which a more complete microscopic model may be built. According to this model, the doping dependences of α_1 and γ_1 arise due to a change in the fraction of SM carriers across the overdoped regime. As mentioned previously, the doping dependence of the T-linear resistivity seemingly sits at odds with an origin rooted in dissipation at a Planckian limit. Nevertheless, if the Planckian scattering is confined to a subset of the carriers, as proposed here, its variation with doping might still be reconciled with the notion of a Planckian bound[8]. The fact that the fall in superfluid density with overdoping also tracks the decrease in the number of SM carriers is intriguing, as it implies that the SC condensate emerges predominantly, if not uniquely, from the ♯3.7 non-FL[49] or non-itinerant[39] sector. Consequently, the suppression of the condensate is seen to be linked directly to the demise of the strange metal and not to a reduction in pairing strength and any associated (disorder-induced) pair-breaking. The reason why α_1, γ_1 and T_c are correlated across the SM regime then becomes apparent.

Methods

High quality Bi2201 and LSCO crystals were grown in floating zone furnaces at 3 different sites. To cover much of the phase diagram, some of the Bi2201 crystals were doped with La and Pb, resulting in the chemical formula: $Bi_{2+z-y}Pb_ySr_{2-x-z}La_xCuO_{6+\delta}$. The Tl2201 crystal studied here was synthesized using a self-flux technique[50]. The hole doping for Bi2201 was estimated from the resistively-measured T_c using the Presland relation[51]: $1 - T_c/T_c^{max} = 82.6(p - 0.16)^2$ with $T_c^{max} = 35$ K. This relation was recently demonstrated to hold well in Bi2201[35]. For LSCO, the doping was estimated from the measured T_c using the same parabolic relation with $T_c^{max} = 38$ K and found to match closely the Sr content of each crystal. The crystallographic axes of LSCO were oriented with a Laue camera. Typical sample dimensions were $1000 \times 250 \times 10\,\mu m^3$ for Bi2201 and Tl2201 and $1500 \times 250 \times 50\,\mu m^3$ for LSCO. The $\rho(0, T)$ curves of all the MR samples are shown in Supplementary Fig. 1.

The MR was measured in DC and pulsed magnets up to 35 T and 70 T, respectively with the current I applied in-plane and $\mathbf{H} \parallel c$. For the pulsed field measurements, samples and wires were fully covered in GE varnish and/or vacuum grease to reduce vibration. To increase the measurement signal, each Bi2201 crystal was mechanically thinned to a thickness of 2–10 μm, resulting in sample resistances of ~1 Ω, i.e. comparable to the resistance of the current contacts. At each measurement temperature, the MR curves were recorded for both polarities of the magnetic field. For Tl2201, a single crystal with an ambient

pressure $T_c = 35$ K was selected and prepared for transport measurements under the application of hydrostatic pressure using a piston cylinder cell. The sample was oriented on a feed-through such that the magnetic field **H** ||*c*. Daphne 7373 oil was used as a pressure transmitting medium as it is known to remain hydrostatic at room temperature (the temperature at which pressure was applied) up to 2.2 GPa[52], beyond the pressures applied in this work.

Data availability

The data that support the findings of this study are available at the University of Bristol data repository, data.bris, at https://doi.org/10.5523/bris.2g87jr92yk2v72t1wz0ynjcsts. Other material is available from the corresponding authors upon request.

References

1. Allen, P. B. The electron-phonon coupling constant λ*. In *Handbook of Superconductivity* (eds. Cardwell, D. A., Larbalestier, D. C. & Braginski, A.) 478–489 (CRC Press, 2000).
2. Kasahara, S. et al. Evolution from non-fermi- to fermi-liquid transport via isovalent doping in $BaFe_2(As_{1-x}P_x)_2$ superconductors. *Phys. Rev. B* **81**, 184519 (2010).
3. Licciardello, S. et al. Electrical resistivity across a nematic quantum critical point. *Nature* **567**, 213–217 (2019).
4. Bruin, J. A. N., Sakai, H., Perry, R. S. & Mackenzie, A. P. Similarity of scattering rates in metals showing *T*-linear resistivity. *Science* **339**, 804–807 (2013).
5. Zaanen, J. Why the temperature is high. *Nature* **430**, 512–513 (2004).
6. Hartnoll, S. A. & Mackenzie, A. P. Planckian dissipation in metals. *Rev. Mod. Phys.* **94**, 041002 (2022).
7. Cooper, R. A. et al. Anomalous criticality in the electrical resistivity of $La_{2-x}Sr_xCuO_4$. *Science* **323**, 603–607 (2009).
8. Legros, A. et al. Universal *T*-linear resistivity and Planckian dissipation in overdoped cuprates. *Nat. Phys.* **15**, 142–147 (2019).
9. Brown, P. T. et al. Bad metallic transport in a cold atom fermi-hubbard system. *Science* **363**, 379 (2019).
10. Cao, Y. et al. Strange metal in magic-angle graphene with near Planckian dissipation. *Phys. Rev. Lett.* **124**, 076801 (2020).
11. Sadovskii, M. Planckian relaxation delusion in metals. *Phys. Uspekhi* **64**, 175–190 (2021).
12. Huang, E. & Das Sarma, S. Linear-in-*T* resistivity in dilute metals: a fermi liquid perspective. *Phys. Rev. B* **99**, 085105 (2019).
13. Patel, A. A. & Sachdev, S. Theory of a Planckian metal. *Phys. Rev. Lett.* **123**, 066601 (2019).
14. Zaanen, J. Planckian dissipation, minimal viscosity and the transport in cuprate strange metals. *SciPost Phys.* **6**, 061 (2019).
15. Yuan, J. et al. Scaling of the strange-metal scattering in unconventional superconductors. *Nature* **602**, 431 (2022).
16. Hussey, N. E., Buhot, J. & Licciardello, S. A tale of two metals: contrasting criticalities in the pnictides and hole-doped cuprates. *Rep. Prog. Phys.* **81**, 052501 (2018).
17. Phillips, P. W., Hussey, N. E. & Abbamonte, P. Stranger than metals. *Science* **377**, eabh4273 (2022).
18. Wu, W., Wang, X. & Tremblay, A. M. S. Non-fermi liquid phase and linear-in-temperature scattering rate in overdoped two-dimensional Hubbard. *Proc. Natl. Acad. Sci. USA* **119**, 15819119 (2022).
19. Seibold, G. et al. Strange metal behaviour from charge density fluctuations in cuprates. *Commun. Phys.* **4**, 7 (2021).
20. Sarkar, T., Mandal, P. R., Poniatowski, N. R., Chan, M. K. & Greene, R. L. Correlation between scale-invariant normal-state resistivity and superconductivity in an electron-doped cuprate. *Sci. Adv.* **5**, eaav6753 (2019).
21. Giraldo-Gallo, P. et al. Scale-invariant magnetoresistance in a cuprate superconductor. *Science* **361**, 479–481 (2018).
22. Ayres, J. et al. Incoherent transport across the strange metal regime of highly overdoped cuprates. *Nature* **595**, 661–667 (2021).
23. Ataei, A. et al. Electrons with Planckian scattering obey standard orbital motion in a magnetic field. *Nat. Phys.* **18**, 1420–1424 (2022).
24. Hussey, N. E., Gordon-Moys, H., Kokalj, J. & McKenzie, R. H. Generic strange-metal behaviour of overdoped cuprates. *J. Phys. Conf. Series* **449**, 012004 (2013).
25. Putzke, C. et al. Reduced Hall carrier density in the overdoped strange metal regime of cuprate superconductors. *Nat. Phys.* **17**, 826–831 (2021).
26. Looney, C. W., Kline, J. E., Mascarenhas, F., Schilling, J. S. & Hermann, A. M. Influence of oxygen content on the activation energy for oxygen ordering in $Tl_2Ba_2CuO_{6+\delta}$. *Physica C* **289**, 203–210 (1997).
27. Pippard, A. *Magnetoresistance in metals.* (Cambridge University Press, 1989).
28. Hinlopen, R. D. H., Ayres, J., Hinlopen, F. A. & Hussey, N. E. B^2 to *B*-linear magnetoresistance due to impeded orbital motion. *Phys. Rev. Res.* **4**, 033195 (2022).
29. Koshelev, A. E. Linear magnetoconductivity in multiband spin-density-wave metals with nonideal nesting. *Phys. Rev. B* **88**, 060412 (2013).
30. Wade, J. M., Loram, J. W., Mirza, K. A., Cooper, J. R. & Tallon, J. L. Electronic specific heat of $Tl_2Ba_2CuO_{6+\delta}$ from 2 K to 300 K for $0 \le \delta \le 0.1$. *J. Supercon.* **7**, 261–264 (1994).
31. Girod, C. *Chaleur Spécifique á Basse Temperature Dans l'état Normal Des Cuprates Superconducteurs*. https://theses.hal.science/tel-03127177 (2021).
32. Grissonnanche, G. et al. Linear-in temperature resistivity from an isotropic Planckian scattering rate. *Nature* **595**, 667–672 (2021).
33. Narduzzo, A. et al. Violation of the isotropic mean free path approximation for overdoped $La_{2-x}Sr_xCuO_4$. *Phys. Rev. B* **77**, 220502 (2008).
34. Ding, Y. et al. Disappearance of superconductivity and a concomitant Lifshitz transition in heavily overdoped $Bi_2Sr_2CuO_6$ superconductor revealed by angle-resolved photoemission spectroscopy. *Chin. Phys. Lett.* **36**, 017402 (2018).
35. Berben, M. et al. On the superconducting dome and pseudogap endpoint in Bi2201. *Phys. Rev. Mater.* **6**, 044804 (2022).
36. Hayes, I. M. et al. Scaling between magnetic field and temperature in the high-temperature superconductor $BaFe_2(As_{1-x}P_x)_2$. *Nat. Phys.* **12**, 916–919 (2016).
37. Abdel-Jawad, M. et al. Anisotropic scattering and anomalous normal-state transport in a high-temperature superconductor. *Nat. Phys.* **2**, 821–825 (2006).
38. Uemura, Y. J. Microscopic phase separation in the overdoped region of high-T_c cuprate superconductors. *Solid State Commun.* **120**, 347–351 (2001).
39. Pelc, D., Popčević, D., Požek, M., Greven, M. & and Barišić, N. Unusual behavior of cuprates explained by heterogeneous charge localization. *Sci. Adv.* **5**, eaau4538 (2019).
40. Li, Z.-X., Kivelson, S. A. & and Lee, D.-H. Superconductor-to-metal transition in overdoped cuprates. *npj Quant. Mat.* **6**, 36 (2021).
41. Tromp, W. O. et al. Puddle formation and persistent gaps across the non-mean-field breakdown of superconductivity in overdoped $(Pb,Bi)_2Sr_2CuO_{6+\delta}$. *Nat. Mat.* **22**, 703–708 (2023).
42. Li, Y. et al. Strongly overdoped $La_{2-x}Sr_xCuO_4$: evidence for Josephson-coupled grains of strongly correlated superconductor. *Phys. Rev. B* **106**, 224515 (2022).
43. Adkins, C. J. Effective-medium theory of conductivity and hall effect in two dimensions. *J. Phys. C: Solid State Phys.* **12**, 3389 (1979).
44. Patel, A. A., McGreevy, J., Arovas, D. P. & Sachdev, S. Magneto-transport in a model of a disordered strange metal. *Phys. Rev. X* **8**, 021049 (2018).

45. Boyd, C. & & Phillips, P. W. Single-parameter scaling in the magnetoresistance of optimally doped $La_{2-x}Sr_xCuO_4$. *Phys. Rev. B* **100**, 155139 (2019).
46. Parish, M. J. & Littlewood, P. B. Non-saturating magnetoresistance in heavily disordered semiconductors. *Nature* **426**, 162–165 (2003).
47. Singleton, J. Temperature scaling behavior of the linear magnetoresistance observed in high-temperature superconductors. *Phys. Rev. Mat.* **4**, 061801 (2020).
48. Hu, J., Parish, M. M. & Rosenbaum, T. F. Nonsaturating magnetoresistance of inhomogeneous conductors: comparison of experiment and simulation. *Phys. Rev. B* **75**, 214203 (2007).
49. Čulo, M. et al. Possible superconductivity from incoherent carriers in overdoped cuprates. *SciPost Phys.* **11**, 012 (2021).
50. Tyler, A. W. J. *An Investigation Into the Magnetotransport Properties of Layered Superconducting Perovskites* (University of Cambridge, 1997).
51. Presland, M. R., Tallon, J. L., Buckley, R. G., Liu, R. S. & Flower, N. E. General trends in oxygen stoichiometry effects on T_c in Bi and Tl superconductors. *Physica* **176C**, 95–105 (1991).
52. Yokogawa, K., Murata, K., Yoshino, H. & Aoyama, S. Pressure transmitting medium Daphne 7474 solidifying at 3. *Jpn. J. Appl. Phys.* **46**, 3636–3639 (2007).

Acknowledgements

We acknowledge stimulating discussions with W. A. Atkinson, P. Chudzinski, P. Coleman, A. Georges, A. Patel and S. Sachdev. We also acknowledge the support of HFML-RU/NWO-I and LNCMI-T, both members of the European Magnetic Field Laboratory (EMFL). This work was supported by the Netherlands Organisation for Scientific Research (NWO) grant No. 16METL01 'Strange Metals' (MB), the European Research Council (ERC) under the European Union's Horizon 2020 research and innovation programme (Grant Agreement No. 835279-Catch-22) (D.J., J.A. and N.E.H.) and the Engineering and Physical Sciences Research Council (UK) grant EP/V02986X/1 (N.E.H.). J.A. acknowledges the support of a Leverhulme Trust Early Career Fellowship. D.V. and C.P. acknowledge support from the EUR grant NanoX no ANR-17-EURE-0009 and from the ANR grant NEPTUN no ANR-19-CE30-0019-01. T.K. acknowledges support from the Asahi Glass Foundation and by the Murata Science Foundation.

Author contributions

The project was conceived and supervised by S.F., A.Ca. and N.E.H. The single crystals were grown by Y.H., T.K. and T.T. The experiments were prepared and performed by J.A., M.B., C.D., Y.-T.H., M.L., I.G., M.M., D.V. and C.P. The data were analysed and figures produced by J.A. and M.B. Supporting Boltzmann modelling was contributed by A.Cu. and R.D.H.H. The manuscript was written by J.A., M.B. and N.E.H. with contributions from all authors.

Competing interests

The authors declare no competing interests.

Additional information

Supplementary information The online version contains supplementary material available at https://doi.org/10.1038/s41467-024-52564-3.

Correspondence and requests for materials should be addressed to J. Ayres or N. E. Hussey.

Peer review information *Nature Communications* thanks the anonymous reviewers for their contribution to the peer review of this work. A peer review file is available.